Investigation of Interlock Geometry Sizes Effect on the Shear Capacity of Dry-Joint Interlocking Core Block Masonry

K. Abdoulaye[1*], D. O. Koteng[2], N. Gathimba[3], R. N. Mutuku[4]

[1]Pan African University Institute for Basic Sciences, Technology and Innovation, hosted at the Jomo Kenyatta University of Agriculture and Technology, Nairobi, Kenya
[2]School of Civil and Resource Engineering, Technical University of Kenya, Nairobi, Kenya
[3]Department of Civil, Construction, and Environmental Engineering, Jomo Kenyatta University of Agriculture and Technology, Kenya
[4]Department of Building and Civil Engineering, Technical University of Mombasa, Kenya

ABSTRACT: Interlocking compressed earth block structure is a dry-stacked system that relies on geometric interlocking rather than mortar. The shear behavior of these structures is linked to the interlock geometry, especially the thickness and depth of the interlocking mechanism. This study examines the in-plane shear behavior of dry-stacked interlocking core block using a finite element triplet shear simulation model in Abaqus, focusing on how interlock thickness and depth influence shear strength, peak displacement, and failure modes. An experimental test was performed with the optimum interlock sizes obtained from the numerical simulation. The results indicate that the shear strength increases with interlock thickness but drops beyond 35mm (11.6% of the block length) due to a significant reduction in the residual soil interface on the female (depression) part. The findings also reveal that changes in interlock thickness have a greater effect on both strength and deformation capacity than changes in interlock depth. Shear strength ranges from 0.08 to 0.25 MPa, representing a 3.1-fold improvement (210% increase) from the thicknesses of 5mm to 35mm (2%-11.6% of the block length). In a similar range of depth, shear strength varies from 0.24 to 0.36 MPa, a 1.5-fold (50% increase) increase. These findings indicate the important role of interlock geometry in the shear performance of dry-stacked joints. The failure mode was characterized by early crushing of the interlock protrusions at thinner thicknesses, whereas at thicker thicknesses, both the interlock protrusions and the residual soil interface on the female face sustained significant damage. These findings emphasize the potential of core interlocking masonry in regions vulnerable to wind and seismic activity.

KEYWORDS: Compressed soil block, Core interlocking block, Dry-stacked joint, Finite element analysis, Interlock depth and thickness, Shear behavior.

[Received: Mar. 03, 2026; Revised: Mar. 08, 2026; Accepted: Mar. 17, 2026] Print ISSN: 0189-9546 | Online ISSN: 2437-2110

I. INTRODUCTION

Masonry structures are among the oldest types of construction. This is mainly due to the availability and low cost of the earthen materials, especially for people with low incomes. The United Nations estimated that the population will reach around 10 billion people in 2050, with 88% residing in developing countries (Ahmad, 2001). This population growth enhances construction needs, requiring more sustainable and affordable materials. Traditional masonry structures consist of linking blocks together with mortar, usually cement-based. The primary conventional masonry weakness under lateral forces is the mortar joints (Bosiljkov et al., 2003), which are vulnerable areas and are further compromised by the disparity between cement mortar and earthen blocks, often resulting in cracks at the mortar interface (Furukawa et al., 2019). Dry-stacked masonry is a masonry system that relies on block-to-block contact to build. Compared to traditional masonry, interlocking block masonry dissipates energy more effectively, which is especially important in seismic regions, as found by (Totoev & Al Harthy, 2016). It also costs less than traditional masonry because it eliminates the need for mortar and speeds up construction. The lack of mortar reduces the amount of cement used, lowering pollution caused by cement manufacturing, cutting costs by 35%, labor by 20% to 40%, and construction time (Dinesh & Rahman, 2022). Several studies (Abdullah et al., 2017; Peng, 2016; Shehu Waziri et al., 2013; Walker, 1995) have shown this sustainability aspect of stabilized interlocking compressed earth blocks, finding that the production of one ton of SICEB generates approximately 22 kg of CO_2, compared to 143 kg for concrete blocks and 200 kg for fired clay bricks. Interlocking masonry units are developed in different shapes, sizes, and interlocking configurations, and are classified either by their geometric design or by their interlocking system. The geometric classification includes interlocking solid blocks (ISBs) and interlocking core blocks (ICBs). The head key (tongue) in ISBs, like the HydraForm type, mainly resists out-of-plane shear loads through interlocking and interface friction, while in-plane shear is opposed mostly through friction (Gul et al., 2022). The protrusions and depressions that constitute the male and female sections on the upper and lower surfaces of interlocking core blocks are key elements in resisting both in-plane and out-of-plane lateral loads (Anand & Ramamurthy, 2005; Bland, 2011; Sturm et al., 2015; Uzoegbo, 2001) and impact shear continuity between masonry layers (Sean Anthony Pringle, 2016). The presence of vertical holes within the ICBs offers several benefits, such as reducing the block's self-weight, improving thermal efficiency, and allowing pipe passage, preventing wall damage from drilling or cutting during

*Corresponding author: abdoulayekarembe18@gmail.com doi: http://dx.doi.org/10.63746/njtd.v23i1.4515

construction. (Baneshi et al., 2023) categorized interlocking blocks based on their interlocking mechanism into four types: trapezoidal, Lego, cross, and checkered types. However, many of the developed systems failed to progress beyond the design phase. The study done by (Anand and Ramamurthy, 2005) reported that several interlocking block systems failed primarily due to complex geometrical configurations that generated stress concentrations at the interlocking protrusions and complicated manufacturing processes. These limitations highlight the need for simpler interlocking geometries, such as the core interlocking Lego block type investigated in this study. The geometry of the interlocking mechanism, acting as shear keys at the head or through protrusions and depressions, is crucial for the wall's shear resistance (Casapulla et al., 2021; Shi et al., 2021; Yousaf et al., 2024) and helps align the wall vertically and horizontally (Saari et al., 2017). The shear capacity of mortarless masonry structures is impacted by the geometry and arrangement of the interlocking mechanism, as well as the frictional forces developed at the interfaces between adjacent unit blocks (Crespi et al., 2016). (Furukawa et al., 2019), found that under lateral in-plane loads, dry-stacked masonry resists mainly through friction activated by confined stress, followed by the strength of the interlocking geometry. The dry-stacked masonry completely collapsed once the interlocking mechanism failed, as supported by the studies of (Nadeem et al., 2023). Their studies on CIB triplet masonry indicated that the middle block slips initially due to the gap between the male and female parts before engaging the interlocking shear keys. From that position, the overall stability of the masonry relies on the interlocking system until failure, highlighting the importance of the design as supported by (Weizmann et al., 2021). In the CIB masonry, too-thin interlock may lead to premature breakage, while too-thick interlock reduces the residual soil interface on the female face, flattening it and mitigating the interlocking shear key effects. Similarly, a deeper interlock increases the risk of early cracking due to the stress concentration, while a shallower depth enhances the risk of unit sliding, especially when the confined stress applied to the masonry wall is lower (Jia & Zhang, 2024; Kasinikota & Tripura, 2024). Despite its advantages, dry-stacked masonry can be risky under lateral forces due to brittle failure from low shear resistance, emphasizing the need to optimize interlock sizes (Elmalyh et al., 2020). While many studies have examined the structural performance of dry-stacked masonry (Dorji et al., 2024; Gul et al., 2022; Han et al., 2020; Khan et al., 2021; Rankawat et al., 2021; Sturm et al., 2015; Yousaf et al., 2024), limited research has focused on how interlocking size affects the in-plane shear behavior (Koudje & Adjovi, 2025), which is critical for low-cost, sustainable materials in seismic zones. Optimizing the interlocking geometry is essential to address constraints between male and female faces and improve shear capacity. To promote wider use, especially in developing countries with limited funds, further research on shear performance is vital to ensure the stability and safety of interlocking compressed earth core block masonry, particularly in earthquake and wind-prone areas. A finite element software, Abaqus, was used to analyze the Triplet shear test, in which core blocks were interlocked with varying interlock geometry sizes. This study investigates the influence of interlock thickness and depth on the in-plane shear behavior of interlocking core block masonry using a numerical simulation model. An experimental testing was conducted with the optimum interlock sizes obtained for validation.

II. Materials and Methods

A. Materials

The block specimen used in this study is a core interlocking compressed earth block. Its dimensions are 300mm x 150mm x 100mm (Length x Width x Height). Two holes of 50mm diameter characterize the block. Each hole is surrounded by the interlock head key that constitutes the protrusion of the male part. To allow blocks to fit together, the depression on the female part is extended by 2mm. The residual soil interface refers to the remaining contact area of the female surface surrounding the interlock cavity that contributes to the shear resistance through friction and compression, as shown in Figure 1. Figure 1 shows the interlocking core block design used in this study.

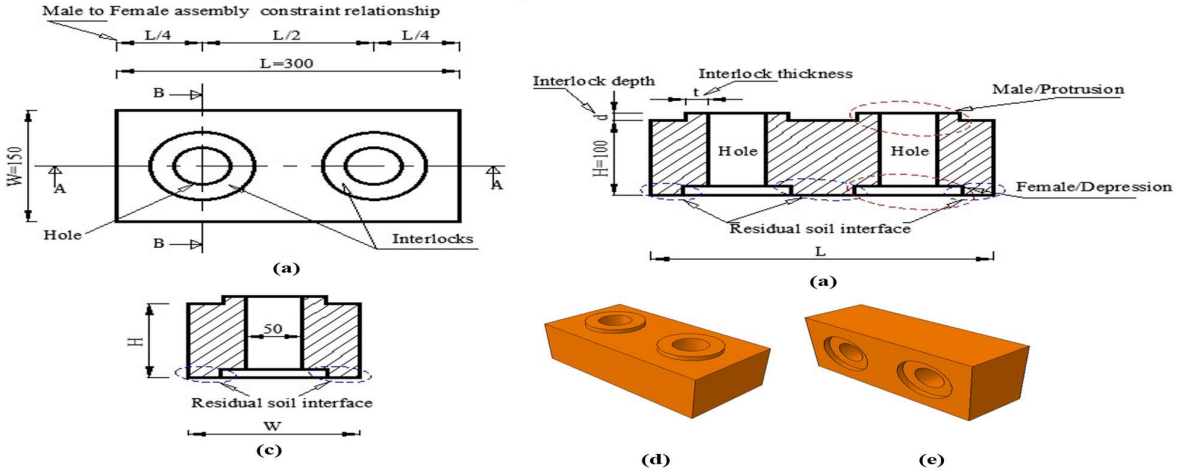

Figure 1 Interlocking Core block design (a)Top view, (b) Section A, (c) Section B, (d) 3D view on male face, (e) 3D view on female face.

B. Methods

1) Finite Element Method

The finite element method (FEM) is a widely used computational technique in engineering for modeling and analyzing complex physical problems (Koudje & Adjovi, 2025). In this study, the FEM was used to simulate the in-plane shear performance of the interlocking core block masonry. The simulations were conducted using Abaqus, a finite element software developed by

Dassault Systèmes that enables the analysis of two-dimensional (2D) and three-dimensional (3D) models under different loading conditions. The numerical simulations incorporated key factors such as material properties, boundary conditions, and loading protocols to realistically reproduce the structural behavior of the masonry assembly. The FEM procedure involves modeling the physical problem, discretizing the domain into finite elements, approximating field variables, assembling the global matrices, and solving the system of equations to obtain stresses and strains within the structure.

2) Experimental program

To complement the numerical analysis, an experimental program was implemented following the triplet shear test method recommended in EN 1052-3 standard (British Standards Institution, 2002). The interlocking blocks were made from locally sourced lateritic soil that was stabilized with 8% Ordinary Portland Cement (OPC) based on the dry weight of the soil. The soil was first characterized to evaluate the basic parameters needed for the numerical study. Before being mixed, the soil was sieved through a 5 mm mesh to remove large particles and ensure consistency in the mixture. The chemical compositions of both the soil and the cement, evaluated through X-Ray Fluorescence (XRF) analysis, are shown in Table 1. After mixing and compaction processes, the blocks were produced and shade-cured under plastic sheeting for 28 days to facilitate proper cement hydration before testing. The unit block was characterized to assess its flexural and compressive capacity before the triplet shear test, as presented in Figure 2. Due to the limited financial resources, the optimum design obtained from the numerical study was molded for practical testing. The experimental triplet samples consisted of three interlocking core blocks stacked together without any mortar joints, representing a dry-joint masonry configuration. Three specimens were tested as required by the standard. The test setup followed the EN 1052-3 standard, where the upper and lower blocks were secured before applying the shear load to the middle block. As recommended by the EN 1052-3 standard, an axial vertical pre-compression stress of 0.1 MPa was applied to the assembly, in addition to the self-weight of the blocks, to simulate the confinement typically present in masonry walls. This axial stress value corresponds to the minimum confinement level recommended by EN 1052-3 standard for masonry units with compressive strength lower than 10 MPa which is consistent with the compressive strength of the interlocking blocks used in this study (5.14 MPa). It was chosen to avoid altering the integrity of the interlocking mechanism before the application of the horizontal lateral load, while still ensuring that the frictional contribution at the block interfaces is properly represented. The horizontal load was applied monotonically, and the resulting shear resistance of the joint was determined from the ratio between the applied horizontal load and the net shear area, corresponding to the two interfaces engaged during lateral loading. The loads were monitored using load cells, while the displacement was measured using linear variable displacement transducers (LVDT). It should be noted that the axial stress was maintained constant throughout the lateral loading, with a maximum variation of ±2% (0.002 MPa), as recommended by the standard. The experimental testing process for the optimum interlocking geometry is illustrated in Figure 2.

Figure 2 Experimental testing process for the optimum interlock sizes.

Table 1 X-Ray Fluorescence of the soil and cement

Chemical components	Al_2O_3	SiO_2	CaO	Fe	Ti	Cl	MgO	P_2O_5	S	K_2O	Mn
Soil (%)	12.9	59.8	1.6	17.6	3.2	1.0	-	-	-	1.0	1.9
Cem I 42.5N (%)	3.8	15.3	70.9	1.9	0.2	0.8	3.7	0.6	2.4	-	-

3) Numerical model

Before the experimental triplet testing, the triplet shear test was numerically simulated in Abaqus following the configuration specified in EN 1052-3 standard (British Standards Institution, 2002). A simplified micro-modeling approach was adopted to represent the dry-joint interlocking masonry assembly composed of three interlocking core blocks. In this study, two steps were required, as illustrated in Figure 3. A first group of nine interlocking thicknesses (5 to 45mm) was simulated with the same interlocking depth of 10mm. The initial depth results are based on the previous study by (Jia & Zhang, 2024). This study investigated interlocking geometries in concrete blocks rather

than compressed earth blocks, their results indicated that shallow allowing uniform transfer of the applied loads. A surface-to-interlock depths around 10 mm were sufficient to initiate surface contact was applied between unit blocks with the mechanical engagement without causing stress concentration. associated parameters obtained during the experimental Therefore, 10 mm was adopted as the initial reference value for characterization of the materials. Similarly to the experimental the present numerical investigation. After obtaining the optimum test procedure, a vertical pre-compression stress of 0.1 MPa, in thickness that provides the maximum shear strength capacity, a addition to the self-weight of the blocks, was applied to the second group of 10 depths (5 to 50mm) was also analyzed using assembly before lateral loading. The lateral load was applied the obtained optimum thickness. This sequential parametric through a monotonic horizontal displacement imposed on a approach was adopted to identify the dominant geometric factors reference point connected to the rigid plate attached to the middle influencing shear capacity while optimizing computational block. A displacement of 10 mm was applied through the efficiency. Although a full factorial design would provide a more reference point (RP) at a loading rate of 0.05 mm/s to robust understanding of interaction effects, this one variable at a progressively capture the development of damage. To ensure time method effectively captures the primary trends of the accurate representation of the stress distribution, a mesh size of masonry shear behavior and serves as a baseline for the research. 2 mm was adopted for the overall block geometry, while a refined The assembly, with overall dimensions of 300 mm x 150 mm x mesh of 0.5 mm was used in the interlocking regions. A mesh 300 mm was restrained at the top and bottom using thick L- convergence analysis confirmed that this configuration provided shaped rigid plates, which were used to apply boundary a better balance between computational accuracy and efficiency, conditions without significantly increasing computational cost. with variations in shear strength within ±2%. Figure 4 presents The interaction between the rigid plates and the blocks was the numerical testing setup and meshing of the triplet assembly. defined using a tie constraint contact, which ensure full displacement compatibility between the contact surfaces and

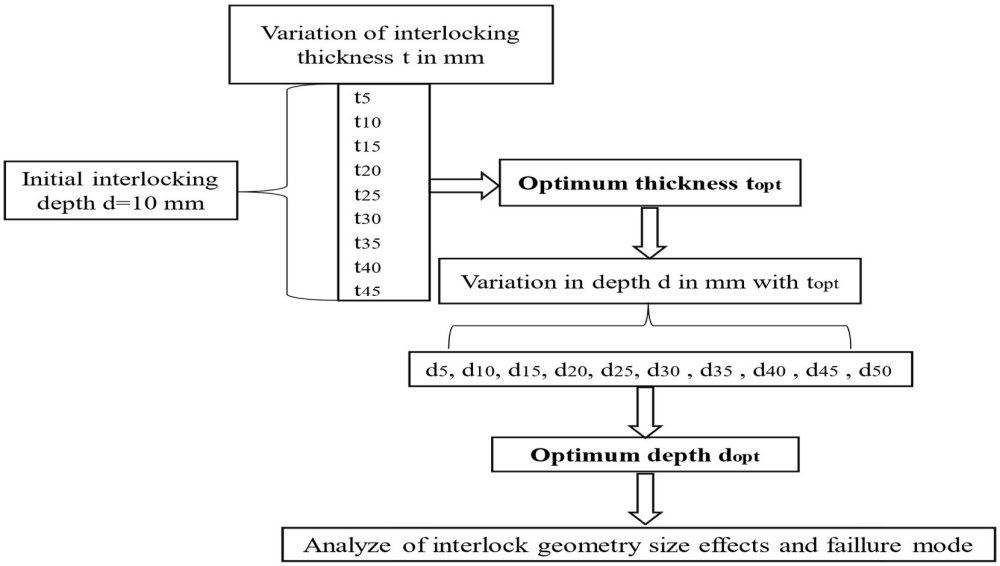

Figure 3 Variation of interlocking geometry sizes for the numerical simulation models

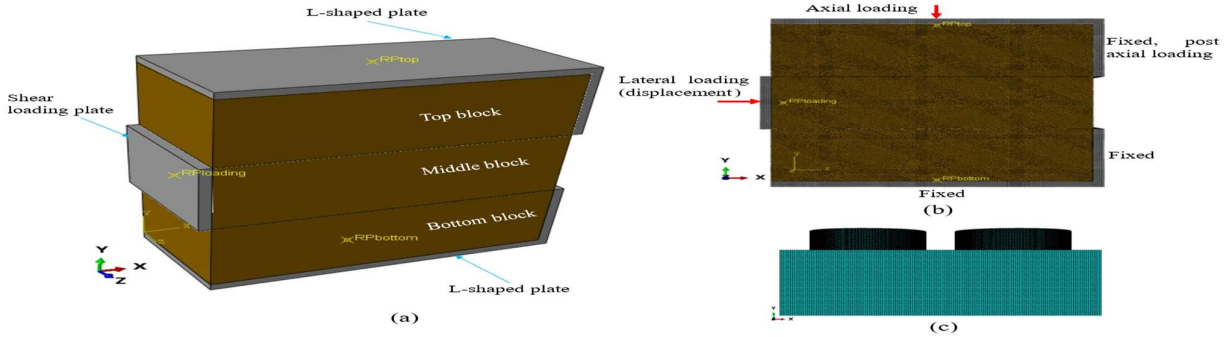

Figure 4 Triplet shear testing model setup, (a) 3D view of the setup; (b) Lateral view of the triplet shear model setup; (c) Lateral view of the unit core block meshing

4) Failure criterion and parameter calibration

The failure criterion of the models was evaluated through the failure of the interlock shear keys. The damage criterion of the masonry was based on the concrete damage plasticity (CDP) model. The fundamental components of the CDP model include three elements: damage progression, yield criterion, and plastic flow rule (Diao et al., 2024). Typically, the nonlinear deformation of quasi-brittle materials is described using the traditional elastic-plastic framework. The total strain in Equation 1 encompasses both elastic and plastic components (Diao et al., 2024).

$$\varepsilon = \varepsilon^{el} + \varepsilon^{Pl} \quad (1)$$

where ε is the overall strain, ε^{el} and ε^{Pl} are, respectively, the elastic and plastic strain. In the CDP constitutive models, nonlinearity results from both plasticity and damage. The material can be damaged by compressive and tensile stresses, leading to crack initiation and reduction in stiffness, when subjected to loading (Diao et al., 2024). The CDP model employs separate damage factors to represent the degradation of stiffness under tensile and compressive loading. The relationship between stress and strain under uniaxial compressive and tensile loads is shown below (Diao et al., 2024).

$$\sigma_c = E\left(\varepsilon_c - \tilde{\varepsilon}_c^{Pl}\right) = (1 - d_c)E_0\left(\varepsilon_c - \tilde{\varepsilon}_c^{Pl}\right) \quad (2)$$

$$\sigma_t = E\left(\varepsilon_t - \tilde{\varepsilon}_t^{Pl}\right) = (1 - d_t)E_0\left(\varepsilon_t - \tilde{\varepsilon}_t^{Pl}\right) \quad (3)$$

Where σ_c and σ_t, are respectively the compressive and tensile stresses, E is the elastic stiffness, E_0 is the initial elastic stiffness, ε_c and ε_t are the total compressive and tensile strain, $\tilde{\varepsilon}_c^{Pl}$ and $\tilde{\varepsilon}_t^{Pl}$ are the equivalent of compressive plastic strain and tensile strain, d_c and d_t, are compressive and tensile damage factors ($0 \leq d_c$ or $d_t \leq 1$) (Diao et al., 2024). The effective compressive and tensile stresses are defined below.

$$\overline{\sigma_c} = \frac{\sigma_c}{(1-d_c)} = E_0\left(\varepsilon_c - \tilde{\varepsilon}_c^{Pl}\right) = E_0\varepsilon_c^{el} \quad (4)$$

$$\overline{\sigma_t} = \frac{\sigma_t}{(1-d_t)} = E_0\left(\varepsilon_t - \tilde{\varepsilon}_t^{Pl}\right) = E_0\varepsilon_t^{el} \quad (5)$$

where $\overline{\sigma_c}$ and $\overline{\sigma_t}$ are the effective compressive and tensile stress, ε_c^{el} and ε_t^{el}, are respectively, the elastic compressive and tensile strains. The general compressive strain can also be separated into the undamaged elastic and the damaged inelastic strain.

$$\varepsilon_c = \tilde{\varepsilon}_c^{in} + \varepsilon_{0c}^{el} \quad (6)$$

$$\varepsilon_{0c}^{el} = \frac{\sigma_c}{E_0} \quad (7)$$

where $\tilde{\varepsilon}_c^{in}$ is the damage inelastic compressive strain, and ε_{0c}^{el}, is the undamaged elastic compressive strain. By applying Equations 4, 6, and 7 to Equation 2, the equivalent compressive plastic strain $\tilde{\varepsilon}_c^{Pl}$, can be formulated as:

$$\tilde{\varepsilon}_c^{Pl} = \varepsilon_c - \varepsilon_c^{el} = \tilde{\varepsilon}_c^{in} - \frac{\sigma_c}{E_0}\frac{d_c}{1-d_c} \quad (8)$$

In the same way, the overall tensile strain is split into the undamaged elastic tensile strain and the tensile strain resulting from damage cracking.

$$\varepsilon_t = \tilde{\varepsilon}_t^{ck} + \varepsilon_{0t}^{el} \quad (9)$$

$$\varepsilon_{0t}^{el} = \frac{\sigma_t}{E_0} \quad (10)$$

where $\tilde{\varepsilon}_t^{ck}$ and ε_{0t}^{el}, are, respectively, the damage-cracking tensile strain and the undamaged elastic tensile strain. By applying Equations 5, 9, and 10 to Equation 1, the equivalent tensile plastic strain $\tilde{\varepsilon}_t^{Pl}$, can be formulated as:

$$\tilde{\varepsilon}_t^{Pl} = \varepsilon_t - \varepsilon_t^{el} = \tilde{\varepsilon}_t^{ck} - \frac{\sigma_t}{E_0}\frac{d_t}{1-d_t} \quad (11)$$

In simulations using the concrete damage plasticity (CDP) model in Abaqus, three key parameters are needed. It includes shear strength, elastic and plastic properties, as well as compressive and tensile properties, as summarized in Tables 2 and 3. The shear strength parameters, including the cohesion and coefficient of friction obtained from the direct shear test on block-to-block interfaces are presented in Table 2. The elastic parameters include Young's modulus and Poisson's ratio. In this study, the elastic modulus and Poisson's ratio were 2100 MPa and 0.25, respectively, based on the experimental characterization of the soil material used. The plastic properties in the concrete damage plasticity model are established, referring to the findings of relevant studies. The expansion angle ψ indicates the volumetric change of the material when subjected to significant inelastic strain (Diao et al., 2024; Rainone et al., 2023). Variations in dilatation angle within the range of 20° to 38° have a lesser effect on the simulation results of stabilized soil materials, as found by (Wosatko et al., 2019). The same study also indicated that an expansion angle value of 30° was found to show high accuracy between the simulation results and experimental data (Wosatko et al., 2019). An initial compressive stress ratio of initial stress ratio f_{b0}/f_{c0} of 1.16, as suggested by (Toutanji, 1999), and the viscosity value of 0.0005, as recommended by (Ali et al., 2021), are used in this study. The eccentricity of 10% and the invariant stress ratio Kc = 0.667, under which the material maintains a relatively stable expansion angle across a broad pressure range, have been used as suggested by (Lubliner et al., 1989). The compressive and tensile behavior parameters used in the Abaqus CDP model are summarized in Table 3. The compressive behavior parameters are derived from the uniaxial compressive test of the stabilized soil specimen. The results obtained give the compressive stress-strain relationship. Alongside Equations 6 and 7, the inelastic strain $\tilde{\varepsilon}_c^{in}$, can be determined. Equation 12 applies the Sidoroff energy-equivalent damage model to calculate the compressive damage factor, d_c (Krajcinovic & Fonseka, 1981). Tensile behavior parameters are obtained through a tensile test of the stabilized soil specimen. The cracking strain ε_t^{ck} was determined using Equations 9 and 10, and the tensile damage factor d_t was determined by using Equation 13. The plastic strains in Equations 8 and 11 have been checked to ensure they are always positive and monotonically increasing, as required by the Abaqus concrete damage plasticity model.

$$d_c = 1 - \sqrt{\frac{\sigma_c}{E_0\varepsilon_c}} \quad (12)$$

$$d_t = 1 - \sqrt{\frac{\sigma_t}{E_0\varepsilon_t}} \quad (13)$$

*Corresponding author: abdoulayekarembe18@gmail.com
doi: http://dx.doi.org/10.63746/njtd.v23i1.4515

Table 2 Shear, elasticity, and plasticity parameters of the specimen used for the study

Shear strength parameters	Friction coefficient/Angle of friction	Cohesion
	0.483/26°	0.178
Elastic parameters	Young modulus	Poisson ratio
	2100 MPa	0.25

Plasticity parameters (Ali et al., 2021; Diao et al., 2024; Lubliner et al., 1989; Rainone et al., 2023; Toutanji, 1999; Wosatko et al., 2019)

Expansion angle	Eccentricity	Initial stress ratio f_{b0}/f_{c0}	Invariant stress ratio K	Coefficient of viscosity
30°	10%	1.16	0.667	$5x10^{-4}$

Table 3 CDP parameters for the compression and tension behavior of the stabilized soil used

σ_c (MP	$\tilde{\varepsilon}_c^{in}$	d_c	σ_t (MP	ε_t^{ck}	d_t
1.520560	0	0	0.51300	0	0
1.726483	0.000058	0	0.472000	0.000243	0.08
2.144589	0.000295	0	0.413000	0.000737	0.19
2.726528	0.000727	0	0.356000	0.001231	0.31
3.308467	0.001136	0	0.285000	0.001731	0.44
3.890408	0.001539	0	0.223000	0.002227	0.57
4.704724	0.001893	0	0.189000	0.002709	0.63
5.08000	0.002245	0	0.135000	0.003201	0.74
4.589797	0.002808	0.09	0.115000	0.003677	0.78
4.007763	0.003375	0.21	0.093000	0.004154	0.82
3.425677	0.004341	0.32	0.046000	0.004643	0.91
2.844587	0.005154	0.44	0.039000	0.005113	0.92
2.257004	0.006228	0.55			
1.681617	0.007435	0.67			
1.105318	0.008686	0.78			
0.515994	0.010352	0.90			

III. RESULTS AND DISCUSSION

This section examines the key results from the numerical simulation of the triplet shear test model. The effect of the interlock thickness and depth on the failure mode and shear strength-displacement behavior of the interlocking masonry is discussed.

A. Effect of interlock geometry sizes on the failure mode

The failure mode was characterized by a crushing of the interlock protrusions for the small thickness values after reaching the peak shear strength. The contact between the protrusion and depression during shear loading results in a concentration of stress at this localized region, as illustrated by the shear contact forces in Figures 5(a) and 5(b). This concentration of stress on the protrusion and the opposite depression indicates the criticality of these regions for interlocking masonry to withstand shear load. With interlock thickness varying between 5 and 30 mm (1.6 to 10% of the block length), the compressive damage variable (d_c) in the protrusion area reached values close to 0.8-0.9. This indicates severe crushing of the shear keys, while the residual soil interface on the female face remained relatively intact ($d_c < 0.2$), as presented in Figures 6(a-c) and 7(a-c) which show the

specific case of 5, 10 and 30mm thickness. From 35 mm to 45 mm of thickness (11.6 to 15% of the block length), damage extended to the residual soil interface, where both tensile (d_t) and compressive (d_c) damage values increased significantly (Figures 6(d-f) and 7(d-f)). This indicates a transition from localized crushing of the protrusions to a more distributed failure involving both the interlock and the surrounding soil interface which serves as the resisting interface for the interlock protrusions during lateral loading, in line with the study by (Hou et al., 2025). Similar failure mode was observed with variation in interlock depth, both with interlock protrusion and with residual soil interface damage. The numerical simulation shows localized damage along the interlocking area, which leads to crack propagation in this region. This behavior is consistent with the experimental result, indicating that the numerical model captures the main failure mechanism of the system as presented in Figures 5 (c) and 5(d).

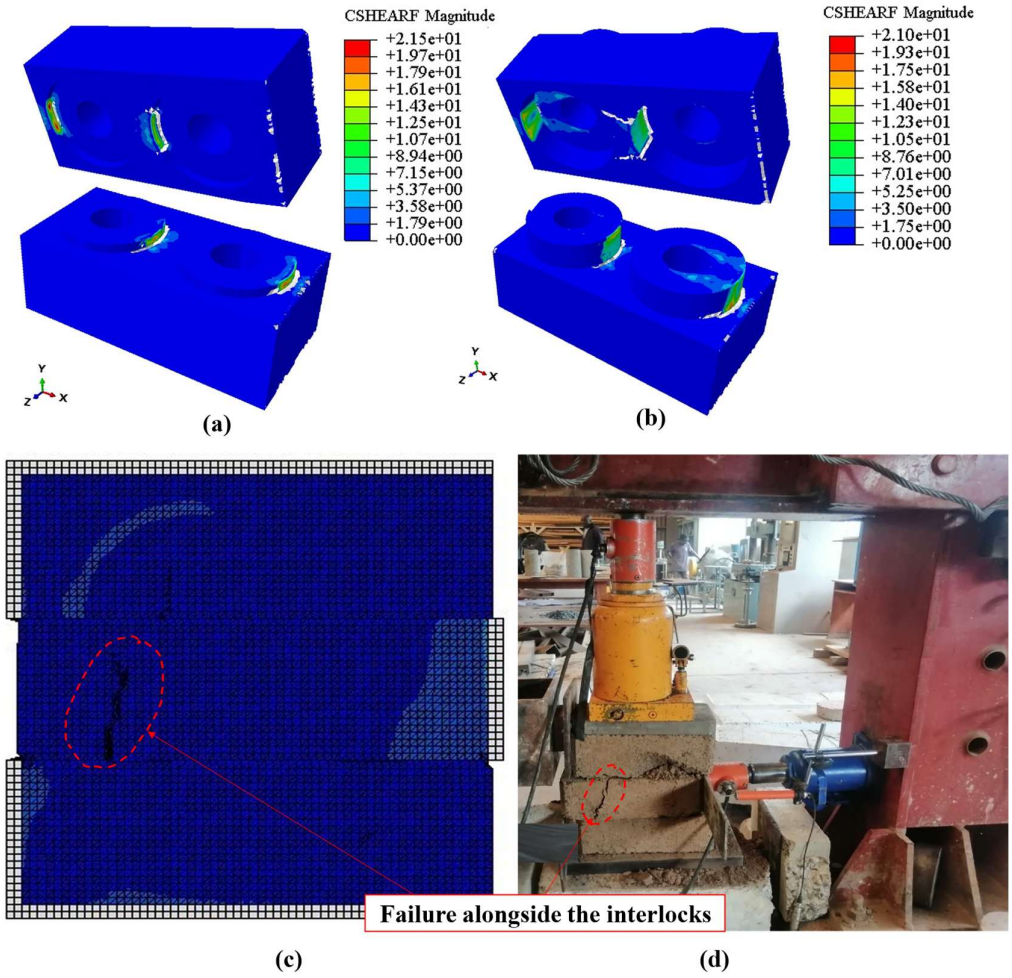

Figure 5 (a) Contact region at the interlock region for 10 mm-depth and optimum thickness, (b) Contact region for optimum depth and thickness, (c) Numerical diagonal failure, (d) Experimental diagonal failure.

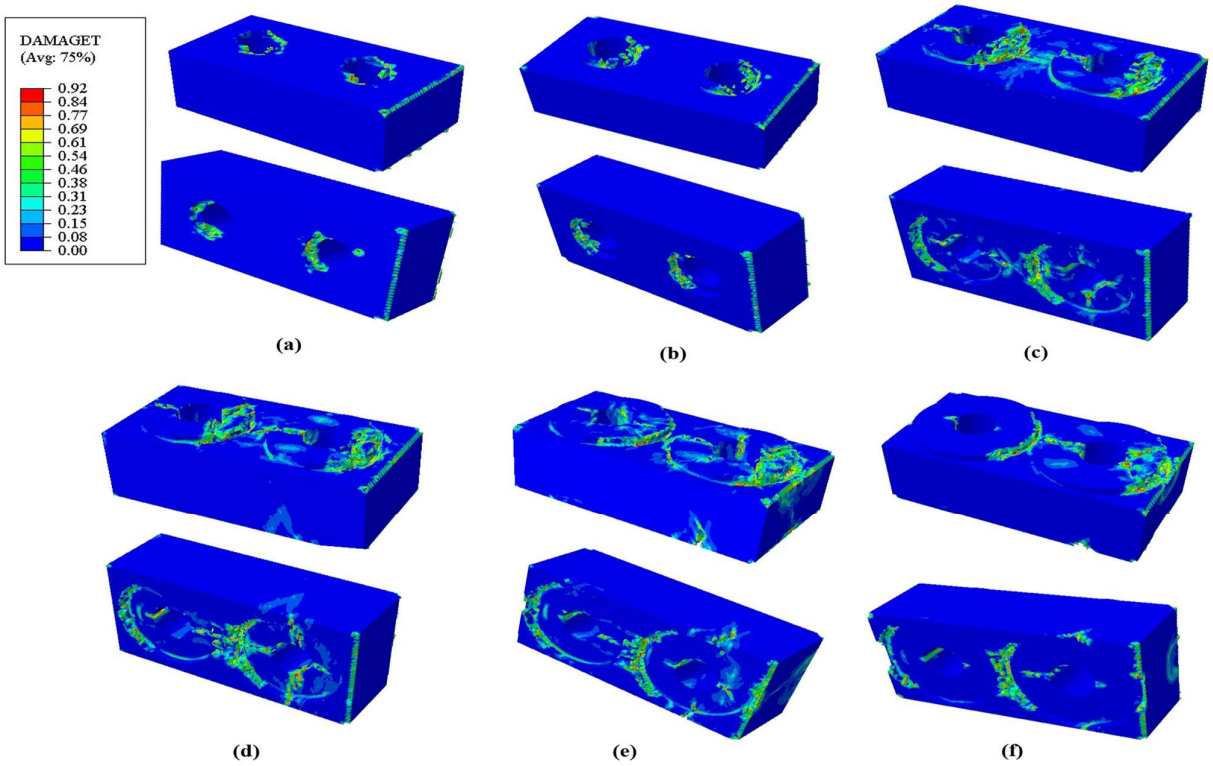

Figure 6 Tensile damage distribution in the middle block's interlock region for varying interlock thicknesses across both male and female faces.

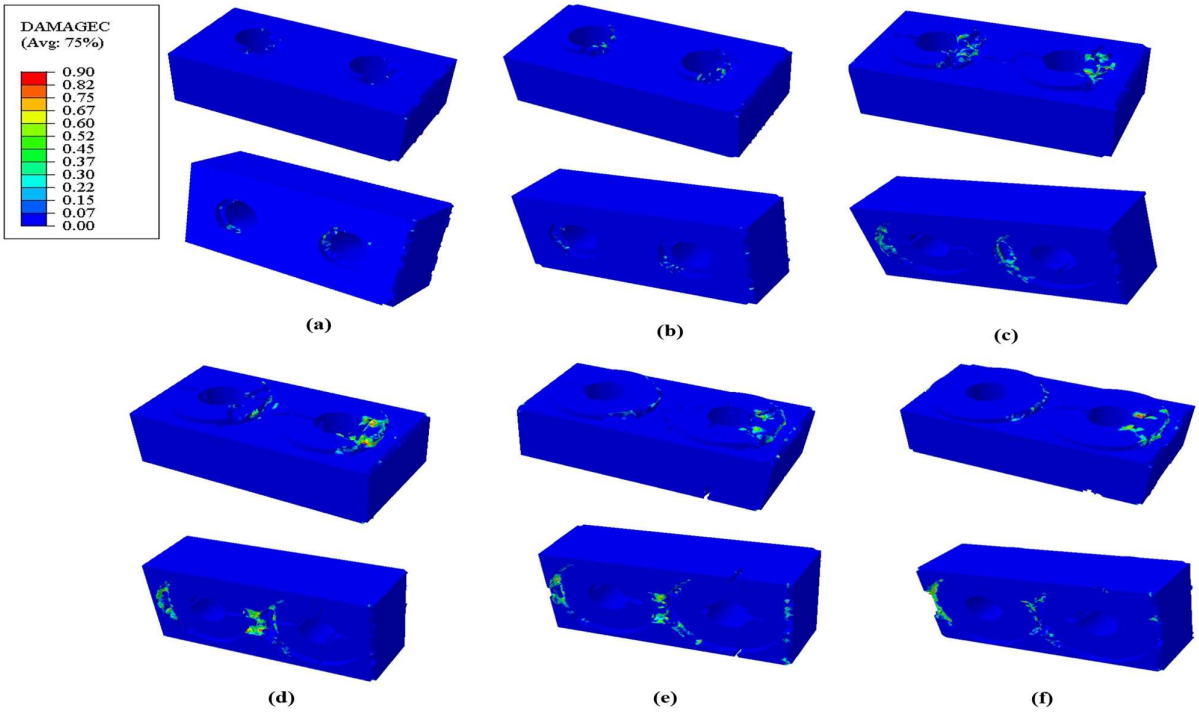

Figure 7 Compressive damage distribution in the middle block's interlock region for varying interlock thicknesses across both male and female faces.

B. Effect of interlock thickness on the shear strength capacity

A series of nine interlocking thicknesses, ranging from 5 to 45mm, with a constant depth of 10mm, was simulated. The corresponding peak shear strengths obtained from the triplet numerical simulations are shown in Figure 8. The flat joint configuration without interlock was primarily modeled as a reference. The shear strength τ_0 given by the reference configuration was 0.080 MPa. For better comparison, the results are expressed in terms of shear ratio τ_i/τ_0, where τ_i is the shear strength (peak value) of the specific interlock size. From Figure 8, a variation in shear strength between 0.080 and 0.081 MPa, corresponding to 2% improvement ($\tau_i/\tau_0 \approx 1.02$) was observed for the thin interlock thickness (thickness of 5 to 10 mm representing 1.6 to 3.3% of the block length). In this region, the protrusion is too thin to provide significant mechanical engagement, and shear transfer is dominated by friction at the flat contact surfaces. The stress fields confirm that only a small portion of the protrusion has been mobilized, resulting in limited improvement in the load-carrying capacity mechanism. With the increase of the interlock thickness to an intermediate value ranging between 15 and 35 mm (5-11.6% of the block length), the shear strength respectively varies from 0.122 to a maximum value of 0.248 MPa. This represents an improvement between 52% and 210% ($\tau_i/\tau_0 = 1.52\ to\ 3.10$) compared to the shear strength given by the reference configuration. This is due to the bearing and dowel action between the male and female parts, enabled by an enlarged interlock area that progressively redistributes and transfers the shear load from pure interface friction to a combination of friction and mechanical interlocking, which explains the noted increase in both stiffness and peak strength of the assembly. This is supported by (Hou et al., 2025) and (Yu et al., 2025), confirming that increasing the geometry of the shear key improves the shear strength capacity of interlocking masonry. The numerical parametric study identified an optimum interlock thickness of 35 mm, yielding a peak shear strength of 0.248 MPa. This value represents a 12% increase over the experimental mean value (τ_{exp} = 0.221 MPa). However, given the experimental coefficient of variation (CoV) of 12% (corresponding to a standard deviation of 0.026 MPa), the numerical prediction falls well within one standard deviation of the experimental results. This close agreement, situated within the experimental scatter (0.198-0.250 MPa), provides a strong indication of the model's validity at this critical design point. Beyond the optimal thickness of 35 mm, the shear strength decreased gradually. The shear strength decreased to 0.194 and 0.175 MPa for thicknesses of 40 and 45mm, respectively, representing 22% and 29% reductions compared to the shear strength at the optimum thickness. This substantial reduction in shear capacity, despite the increase in interlock contact areas, is explained by the significant decrease in the residual soil interface region on the female part. It is also important to note that between thicknesses of 30 mm and 35 mm, only a 2.25% increase was observed, indicating a stagnation in shear capacity in this region.

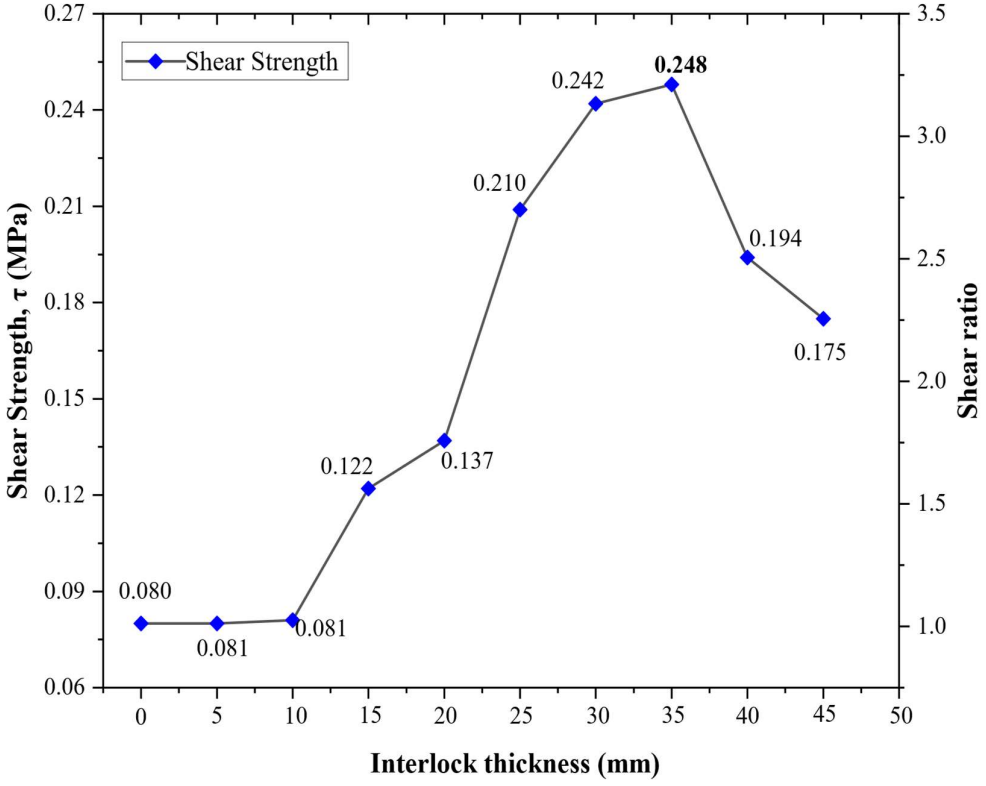

Figure 8 Variation of the shear strength with the interlock thickness (depth 10mm)

*Corresponding author: abdoulayekarembe18@gmail.com
doi: http://dx.doi.org/10.63746/njtd.v23i1.4515

The peak displacement for each interlock thickness is presented in Figure 9. The results show that interlock thickness affects the deformation capacity of the dry-stacked joint. The peak displacement in the reference configuration remains relatively small due to the lack of an interlocking mechanism, which usually provides additional resistance to sliding. A net improvement was observed with the addition of the interlock. Compared to the reference configuration's peak displacement, the peak displacement for the small interlock (5 and 10mm) was on average 2.7 times higher, while 3.5 times higher for the thickness ranging between 15 and 20mm. From a 25mm-thickness, a stabilization of the peak displacement was observed with a maximum value of 3.18mm. This is explained by the interlock's stiffness and the sufficient resistance of the residual soil interface on the female part. Beyond 35mm of thickness, a light decrease (7% to 13%) in displacement was observed. This reduction, despite the increase in interlock thickness, is associated with a decrease in the residual soil interface on the female part, resulting in thin webs that can lead to early splitting and localized cracking.

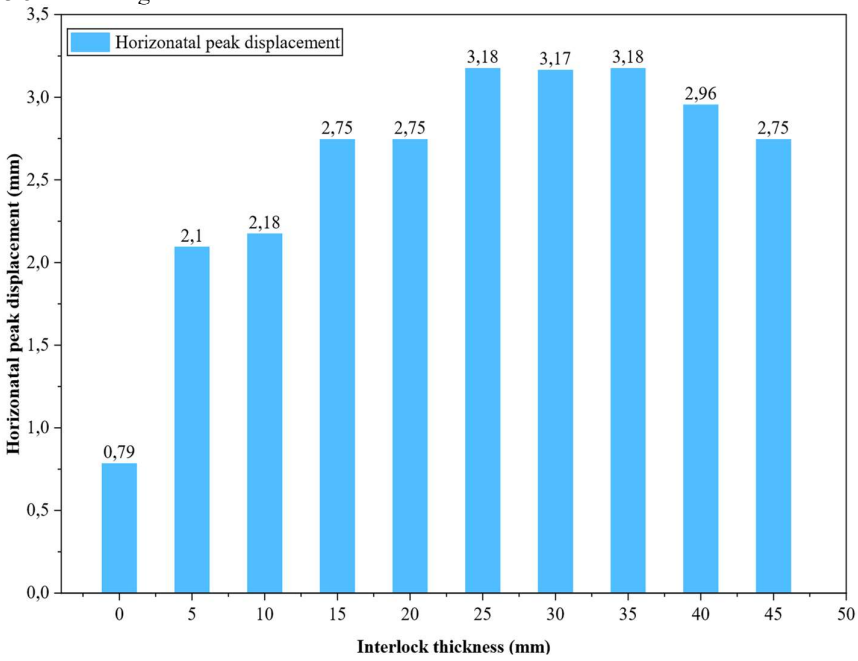

Figure 9 Peak displacement curve with interlock thickness (depth 10mm)

C. Effect of interlocking depth on the shear capacity

After identifying the optimum interlock thickness of 35mm, this value was kept constant, and the interlock depth was varied from 5 to 50mm (half height of the block). The results indicate a significant influence of interlock depth on the shear strength capacity, but no significant influence on the peak displacement. Figure 10 represents the peak shear strength with the variation of the interlock depth. The introduction of a small interlock depth of 5mm with the optimum thickness gave a net improvement in shear strength compared to the reference configuration (flat joint). The shear strength of the 5mm depth gave a peak value of 0.244 MPa, corresponding to an increase of 205% compared to the reference configuration ($\tau_i/\tau_0 = 3.05$). A similar value is obtained at a 10 mm depth (0.248 MPa, +210%), showing that the simple presence of a shear key with a small protrusion (5 to 10% of the block height) significantly increases shear strength capacity by a factor of 3 compared to the flat joint capacity. As the depth is further increased from 15 to 35 mm, the shear strength capacity continues to monotonically increase from 0.277 to 0.356 MPa, corresponding to a shear ratio between 3.46 and 4.45 (246 to 345% increase). This finding is supported by the study done by (Baneshi et al., 2023), indicating that a larger interlock contact area can enhance the overall shear capacity of a dry-stacked structure. The optimum shear value of the shear strength was found for a depth of 35 mm. This is explained by the deeper engagement of the protrusion-depression system, which enlarges the effective shear-transfer area and extends the internal stress throughout the blocks. The shear strength capacity slightly dropped to 0.347, 0.333, and 0.315 MPa for depths of 40, 45, and 50 mm, respectively. This reduction in shear strength (3 to 12%) at large depths (40 to 50% of the block depth) indicates that the material surrounding the interlock on the female part becomes more heavily stressed, leading to a reduction in shear strength. The peak displacements were stable and showed an increase of around 0.02% in average compared to the peak displacement at a depth of 5mm. This indicates that the interlock depth affects shear strength more than it affects peak displacement, as supported by (Jia & Zhang, 2024). The peak displacement value for each interlock depth and the variation ratio is summarized in Table 4.

*Corresponding author: abdoulayekarembe18@gmail.com
doi: http://dx.doi.org/10.63746/njtd.v23i1.4515

Table 4 Peak displacement with interlock depth variation

Interlock depth (mm)	Peak displacement (mm)	Increase ratio (%)
5	3.1793	0
10	3.1801	0.03
15	3.1802	0.03
20	3.1800	0.02
25	3.1797	0.02
30	3.1801	0.03
35	3.1800	0.02
40	3.1795	0.01
45	3.1794	0.01
50	3.1798	0.01

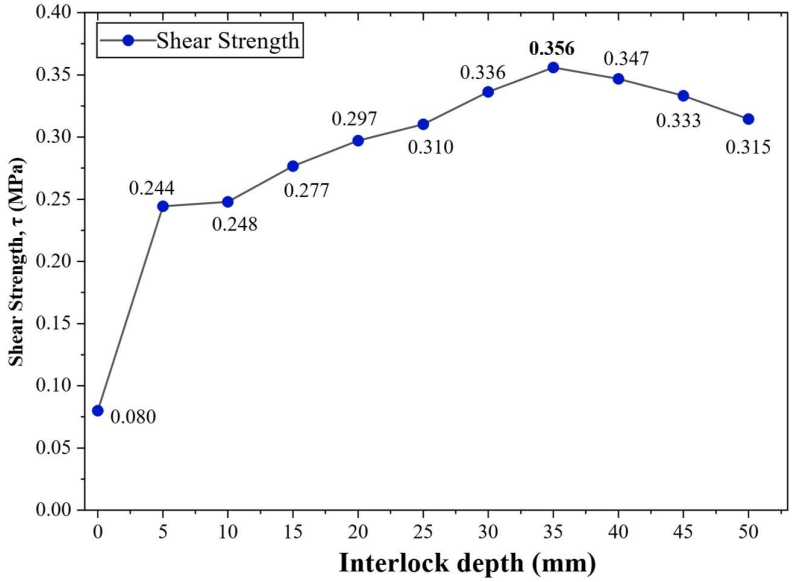

Figure 10 Variation of the shear strength with the interlock depth (optimum thickness 35mm)

The variation in interlock thickness significantly affects both strength and deformation capacity, compared with the variation in interlock depth. The shear strength varies from 0.081 to 0.248 MPa, corresponding to approximately a 3.1-fold increase from 5 mm to 35 mm in thickness. While it varies from 0.244 to 0.356 MPa within the same depth range, representing a 1.5-fold improvement. This indicates that the variation in interlock depth has a 50% lower effect than the variation in interlock thickness within the same range. These results indicate a significant influence of interlock geometry on the shear performance of dry-stacked joints.

IV. CONCLUSION

This study investigates the influence of interlock depth and thickness on the shear behavior of interlocking compressed soil core block structures using a numerical triplet shear test. The shear strength capacity of the assembly increases with interlock thickness, peaking at 35 mm (11.6% of block length) before declining by 22% at 40 mm (13.3% of block length). Variation in interlock thickness affects shear strength four times more than variation in interlock depth across the same range. Peak displacement increases with thickness, stabilizing between 25 and 35 mm (8.3–11.6% of block length) before a slight decrease beyond 35 mm, with only 0.02% variation observed; interlock depth showed a lesser effect on deformation capacity. The combination of 35 mm thickness and depth—representing 11.6% of block length and 35% of block height—yielded the highest shear strength at 0.356 MPa. Failure mode analysis revealed that thin protrusions failed through rapid deletion due to early cracking, whereas thicker, deeper interlocks caused more severe damage to the residual soil interface on the female face due to stress concentration.

Future research could examine the combined effect of interlock geometry and full block dimensions on shear capacity, including the development of a predictive model that incorporates interlock size parameters for core-interlocking block masonry. While this study identified an optimal geometry through sequential analysis, subsequent investigations should employ a full factorial design to capture potential synergistic interactions between thickness and depth, thereby identifying a global optimum. Such work

would enhance understanding of interlocking core block masonry behavior and support its application as a low-cost, sustainable housing solution in regions with limited financial resources, particularly in developing countries.

REFERENCES

Abdullah, A. H., Nagapan, S., Antonyova, A., Rasiah, K., Yunus, R., & Sohu, S. (2017). Strength and Absorption Rate of Compressed Stabilized Earth Bricks (CSEBs) Due to Different Mixture Ratios and Degree of Compaction. MATEC Web of Conferences, 103, 01028. https://doi.org/10.1051/matecconf/201710301028

Ahmad, K. (2001). Global population will increase to nine billion by 2050, says UN report. The Lancet, 357(9259), 864. https://doi.org/10.1016/S0140-6736(05)71800-6

Ali, O., Abbas, A., Khalil, E., & Madkour, H. (2021). Numerical investigation of FRP-confined short square RC columns. Construction and Building Materials, 275, 122141. https://doi.org/10.1016/j.conbuildmat.2020.122141

Anand, K. B., & Ramamurthy, K. (2005). Development and Evaluation of Hollow Concrete Interlocking Block Masonry System. The Masonry Society Journal, 23(1). https://doi.org/10.70803/001c.130934

Baneshi, V., Dehghan, S. M., & Hassanli, R. (2023). An experimental study on the behavior of interlocking masonry blocks manufactured using 3D printed mold. Advances in Structural Engineering, 26(2), 360–380. https://doi.org/10.1177/13694332221126595

Bland, D. W. (2011). In-plane cyclic shear performance of interlocking compressed earth block walls. Thesis, Faculty of California Polytechnic State University, San Luis Obispo.

Bosiljkov, V., A. W. Page, V. Bokan-Bosiljkov, & R. Zarnic. (2003). Performance Based Studies of in-Plane Loaded Unreinforced Masonry. Masonry International, 16, 39–50.

Modena, C., Da Porto, F., & Valluzzi, M. R. (2016). Brick and block masonry: Proceedings of the 16th international brick and block masonry conference, padova, italy, 26-30 june 2016. CRC Press. https://doi.org/10.1201/b21889

British Standard Institution. (2002). BS EN 1052-3. Methods of test for masonry-Part, 3.

Casapulla, C., Mousavian, E., Argiento, L., Ceraldi, C., & Bagi, K. (2021). Torsion-shear behaviour at the interfaces of rigid interlocking blocks in masonry assemblages: experimental investigation and analytical approaches. Materials and Structures, 54(3), 134. https://doi.org/10.1617/s11527-021-01721-x

Crespi, P., Sturm, T., Formisano, A., De, J., & Ortúzar, D. (2016). Experimental and numerical study of partially grouted reinforced masonry shear walls subjected to in-plane loading Sebastián Andrés Calderón Díaz.

Diao, Y., Yan, Y., Zheng, G., Wang, Z., Yu, H., & Huang, J. (2024). Mechanical properties and damage plastic model for cement-soil mortar: Laboratory tests and numerical analysis. Case Studies in Construction Materials, 21, e03957. https://doi.org/10.1016/j.cscm.2024.e03957

Dinesh, R. G., & Rahman, S. S. A. (2022). Analytical investigation on interlocking brick masonry with RC frame. International Journal of Health Sciences, 5929–5939. https://doi.org/10.53730/ijhs.v6nS5.10004

Dorji, S., Derakhshan, H., Thambiratnam, D. P., & Mohyeddin, A. (2024). Lateral load response of semi-interlocking mortarless masonry-infilled frames. Structures, 61, 105998. https://doi.org/10.1016/j.istruc.2024.105998

Elmalyh, S., Bouyahyaoui, A., Cherradi, T., Rotaru, A., & Mihai, P. (2020). In-Plane Shear Behavior of Unreinforced Masonry Walls Strengthened with Fiber Reinforced Polymer Composites. Advances in Science, Technology and Engineering Systems Journal, 5(2), 360–367. https://doi.org/10.25046/aj050247

Furukawa, A., Prasetyo, J. J., & Kiyono, J. (2019). Failure process and load-displace-ment relationship of rectangular block and interlocking block walls during in-plane lateral loading Failure process and load-displacement relationship of rectangular block and interlocking block walls during in-plane lateral loading. https://doi.org/https://doi.org/10.24762/jndsj.38.S06_25

Gul, A., Alam, B., & Shahzada, K. (2022). Seismic performance evaluation of unconfined dry stacked block masonry structure. Engineering Structures, 265, 114529. https://doi.org/10.1016/j.engstruct.2022.114529

Han, L. C., Bin Mirasa, A. K., Saad, I., Bt. Bolong, N., Bt. Asman, N. S. A., Bte Asrah, H., & Bin Abdullah, E. S. R. (2020). Use of Compressed Earth Bricks/Blocks in Load-Bearing Masonry Structural Systems: A Review. Materials Science Forum, 997, 9–19. https://doi.org/10.4028/www.scientific.net/MSF.997.9

Hou, Y., Liu, D., Qi, D., Liu, S., Wang, T., & Zhang, J. (2025). Shear Behavior of Large Keyed Dry Joints in Segmental Precast Bridges: Experiment, Numerical Modeling, and Capacity Prediction. Buildings, 15(18), 3375. https://doi.org/10.3390/buildings15183375

Jia, L., & Zhang, D. (2024). Numerical simulation research on the influence of interlocking depth and block number on the compressive performance of interlocking block masonry. Applied Mathematics and Nonlinear Sciences, 9(1). https://doi.org/10.2478/amns-2024-1499

Kasinikota, P., & Tripura, D. D. (2024). Shear capacity of interlocking compressed stabilized earth block masonry panels. European Journal of Environmental and Civil Engineering. https://doi.org/10.1080/19648189.2024.2372611

Khan, I., Gul, A., Shahzada, K., Khan, N. A., Rehman, F. U., Samiullah, Q., & Khattak, M. A. (2021). Computational Seismic Analysis of Dry-Stack Block Masonry Wall. Civil Engineering Journal, 7(3), 488–501. https://doi.org/10.28991/cej-2021-03091668

Koudje, B., & Adjovi, E. (2025). Numerical Simulation of a Shear Wall Model in Interlocking Masonry with Dry Vertical and Horizontal Joints in Compressed Earth Blocks. Buildings, 15(4), 627. https://doi.org/10.3390/buildings15040627

Krajcinovic, D., & Fonseka, G. U. (1981). The Continuous Damage Theory of Brittle Materials, Part 1: General Theory. Journal of Applied Mechanics, 48(4), 809–815. https://doi.org/10.1115/1.3157739

Lubliner, J., Oliver, J., Oller, S., & Oñate, E. (1989). A plastic-damage model for concrete. International Journal of Solids and Structures, 25(3), 299–326. https://doi.org/10.1016/0020-7683(89)90050-4

Nadeem, M., Gul, A., Bahrami, A., Azab, M., Khan, S. W., & Shahzada, K. (2023). Evaluation of mechanical properties of cored interlocking blocks – A step toward affordable masonry material. Results in Engineering, 18, 101128. https://doi.org/10.1016/j.rineng.2023.101128

Peng, C. (2016). Calculation of a building's life cycle carbon emissions based on Ecotect and building information modeling. Journal of Cleaner Production, 112, 453–465. https://doi.org/10.1016/j.jclepro.2015.08.078

Rainone, L. S., Tateo, V., Casolo, S., & Uva, G. (2023). About the Use of Concrete Damage Plasticity for Modeling Masonry Post-Elastic Behavior. Buildings, 13(8), 1915. https://doi.org/10.3390/buildings13081915

Rankawat, N., Brzev, S., Jain, S. K., & Pérez Gavilán, J. J. (2021). Nonlinear seismic evaluation of confined masonry structures using equivalent truss model. Engineering Structures, 248, 113114. https://doi.org/10.1016/j.engstruct.2021.113114

Saari, S., Bakar, B. H. A., & Surip, N. A. (2017). Strength properties of interlocking compressed earth brick units. 020017. https://doi.org/10.1063/1.5005648

Sean Anthony Pringle. (2016). Diagonal Tension Testing of Interlocking Compressed Earth Block Panels. Master Thesis, Faculty of California Polytechnic State University, San Luis Obispo.

Shehu Waziri, B., Alhaji Lawan, Z., & Mala, Aji. (2013). Properties of Compressed Stabilized Earth Blocks (CSEB) For Low-Cost Housing Construction: A Preliminary Investigation. In International Journal of Sustainable Construction Engineering & Technology (Vol. 4, Number 2). http://penerbit.uthm.edu.my/ojs/index.php/IJSCET

Shi, T., Zhang, X., Hao, H., & Chen, C. (2021). Experimental and numerical investigation on the compressive properties of interlocking blocks. Engineering Structures, 228, 111561. https://doi.org/10.1016/j.engstruct.2020.111561

Sturm, T., Ramos, L. F., & Lourenço, P. B. (2015). Characterization of dry-stack interlocking compressed earth blocks. Materials and Structures, 48(9), 3059–3074. https://doi.org/10.1617/s11527-014-0379-3

Totoev, Y., & Al Harthy, A. (2016). Semi Interlocking Masonry as Infill Wall System for Earthquake Resistant Buildings: A Review. The Journal of Engineering Research, 15(2), 33. https://doi.org/10.24200/tjer.vol13iss1pp33-41

Toutanji, H. (1999). Stress-Strain Characteristics of Concrete Columns Externally Confined with Advanced Fiber Composite Sheets. ACI Materials Journal, 96(3), 397–404. https://doi.org/https://doi.org/10.14359/639

Uzoegbo, H. C. (2001). Lateral Loading Tests on Dry-Stack Interlocking Block Walls. In Structural Engineering, Mechanics and Computation (pp. 427–436). Elsevier. https://doi.org/10.1016/B978-008043948-8/50044-8

Walker, P. J. (1995). Strength, durability and shrinkage characteristics of cement stabilised soil blocks. Cement and Concrete Composites, 17(4), 301–310. https://doi.org/10.1016/0958-9465(95)00019-9

Weizmann, M., Amir, O., & Grobman, Y. J. (2021). The effect of block geometry on structural behavior of topological interlocking assemblies. Automation in Construction, 128, 103717. https://doi.org/10.1016/j.autcon.2021.103717

Wosatko, A., Winnicki, A., Polak, M. A., & Pamin, J. (2019). Role of dilatancy angle in plasticity-based models of concrete. Archives of Civil and Mechanical Engineering, 19(4), 1268–1283. https://doi.org/10.1016/j.acme.2019.07.003

Yousaf, S. M., Gul, A., Shahzada, K., & Khan, S. W. (2024). Evaluation of lateral strength capacity of cored interlocking block masonry piers under variable pre-compression loads. Structures, 70, 107640. https://doi.org/10.1016/j.istruc.2024.107640

Yu, F., Jiang, Q., Chong, X., Zhang, L., Huang, J., & Feng, Y. (2025). Investigation of the shear performance of multi-key block bonding surfaces without connecting reinforcement for precast elements. Scientific Reports, 15(1), 40274. https://doi.org/10.1038/s41598-025-24057-w